

SH3YL1 regulates dorsal ruffle formation by a novel phosphoinositide-binding domain

Junya Hasegawa,¹ Emi Tokuda,² Takeshi Tenno,³ Kazuya Tsujita,² Haruko Sawai,¹ Hidekazu Hiroaki,³ Tadaomi Takenawa,² and Toshiki Itoh¹

¹Division of Membrane Biology, ²Division of Lipid Biochemistry, and ³Division of Structural Biology, Department of Biochemistry and Molecular Biology, Kobe University Graduate School of Medicine, Kobe, Hyogo 650-0017, Japan

Reversible interactions between cytosolic proteins and membrane lipids such as phosphoinositides play important roles in membrane morphogenesis driven by actin polymerization. In this paper, we identify a novel lipid-binding module, which we call the SYLF domain (after the SH3YL1, Ysc84p/Lsb4p, Lsb3p, and plant FYVE proteins that contain it), that is highly conserved from bacteria to mammals. SH3YL1 (SH3 domain containing Ysc84-like 1) strongly bound to phosphatidylinositol 3,4,5-triphosphate (PI(3,4,5)P₃) and several D5-phosphorylated phosphoinositides through its SYLF domain and was localized to circular dorsal ruffles induced

by platelet-derived growth factor stimulation. Interestingly, SHIP2 (the PI(3,4,5)P₃ 5-phosphatase, src-homology 2-containing inositol-5-phosphatase 2) was identified as a binding partner of SH3YL1, and knockdown of these proteins significantly suppressed dorsal ruffle formation. Phosphatidylinositol 3,4-bisphosphate (PI(3,4)P₂), which is mainly synthesized from PI(3,4,5)P₃ by the action of SHIP2, was enriched in dorsal ruffles, and PI(3,4)P₂ synthesis strongly correlated with formation of the circular membrane structure. These results provide new insight into the molecular mechanism of dorsal ruffle formation and its regulation by phosphoinositide metabolism.

Introduction

Membrane ruffles are short-lived, highly dynamic, and F-actin-enriched structures induced by various extracellular stimuli. It is now well established that treatment with growth factors, including EGF and PDGF, results in the formation of two different types of plasma membrane structures: peripheral ruffles and dorsal ruffles (Buccione et al., 2004). Of these two structures, dorsal ruffles are easily distinguishable from peripheral ruffles by their unique ring-shaped morphology and are believed to play important roles in the establishment of polarity in motile cells, macropinocytosis, and the internalization of cell surface receptors (Dowrick et al., 1993; Warn et al., 1993; Swanson and Watts, 1995; Krueger et al., 2003; Orth and McNiven, 2006). For the formation of dorsal ruffles, engagement of the growth factors to their receptor tyrosine kinases activates early effector kinases such as phosphatidylinositol 3-kinase (PI3K) and Src. This leads to the activation of downstream signaling proteins, including small GTPases such as

Rac, Ras, and Rab5 and serine/threonine kinases such as protein kinase A and Pak1 (Dharmawardhane et al., 2000; Lanzetti et al., 2004; Palamidessi et al., 2008). Consequently, these signaling pathways are thought to regulate the activity of cytoskeletal components such as neuronal Wiskott-Aldrich syndrome protein (N-WASP), Arp2/3, cortactin, sorting nexin 9, and dynamin for the robust actin polymerization at dorsal ruffles (Krueger et al., 2003; Buccione et al., 2004; Legg et al., 2007; Yarar et al., 2007). Despite these findings, the role of membrane lipids such as phosphoinositides and their metabolizing enzymes, including phosphoinositide kinases and phosphatases, is yet to be determined.

Reversible interactions between soluble cytosolic proteins and phospholipids in the plasma membrane are essential for a wide variety of cellular functions, including vesicular trafficking, cell proliferation, and motility (Itoh and Takenawa, 2002; Lemmon, 2008). Moreover, studies in recent years have revealed that the curvature of membranes can be determined by a certain group of lipid-binding modules such as Bin-Amphiphysin-Rvs (BAR), Fer-CIP4 homology and BAR (F-BAR), and Epsin N-terminal

Correspondence to Toshiki Itoh: titoh@med.kobe-u.ac.jp

Abbreviations used in this paper: BAR, Bin-Amphiphysin-Rvs; CBB, Coomassie brilliant blue; ENTH, Epsin N-terminal homology; N-WASP, neuronal Wiskott-Aldrich syndrome protein; PC, phosphatidylcholine; PE, phosphatidylethanolamine; PH, pleckstrin homology; PI(3,4)P₂, phosphatidylinositol 3,4-bisphosphate; PI(3,4,5)P₃, phosphatidylinositol 3,4,5-triphosphate; PI3K, phosphatidylinositol 3-kinase; SVM, support vector machine.

© 2011 Hasegawa et al. This article is distributed under the terms of an Attribution-Noncommercial-Share Alike-No Mirror Sites license for the first six months after the publication date (see <http://www.rupress.org/terms>). After six months it is available under a Creative Commons License (Attribution-Noncommercial-Share Alike 3.0 Unported license, as described at <http://creativecommons.org/licenses/by-nc-sa/3.0/>).

homology (ENTH) domains (McMahon and Gallop, 2005; Itoh and De Camilli, 2006; Heath and Insall, 2008). These domains not only bind to acidic phospholipids but can also transform PI(4,5)P₂-containing liposomes into elongated membrane tubules in vitro (Takei et al., 1999; Farsad et al., 2001; Ford et al., 2002; Itoh et al., 2005; Tsujita et al., 2006). In addition, overexpression of these domains can also induce robust tubular invaginations of the plasma membrane in the cell (Lee et al., 2002; Kamioka et al., 2004). The BAR domain super family proteins, including those with the BAR and F-BAR domains, typically contain a single or tandem SH3 domains at their C termini to form a molecular complex with N-WASP and dynamin, two key components in actin polymerization and membrane fission during clathrin-mediated endocytosis (Ringstad et al., 1997; Itoh et al., 2005; Tsujita et al., 2006).

Here, we describe a novel phosphoinositide-binding domain in a group of proteins with a C-terminal SH3 domain named the SYLF (SH3YL1, Ysc84p/Lsb4p, Lsb3p, and plant FYVE protein) domain. The SYLF domain of an SH3 domain containing Ysc84-like 1 (SH3YL1), a mammalian protein, strongly binds to D5-phosphoinositides including phosphatidylinositol 3,4,5-triphosphate (PI(3,4,5)P₃). We further identify the PI(3,4,5)P₃ 5-phosphatase src-homology 2-containing inositol-5-phosphatase 2 (SHIP2) as a binding partner for SH3YL1, and both proteins are required for the formation of circular dorsal ruffles induced by PDGF stimulation. Phosphatidylinositol 3,4-bisphosphate (PI(3,4)P₂), which is synthesized from PI(3,4,5)P₃ by the action of SHIP2, is enriched at matured dorsal ruffles, indicating that this phosphoinositide transition plays an important role in the formation of the ring-shaped membrane structure. Our findings suggest a mechanism by which SH3YL1 couples SHIP2 as well as subsequent PI(3,4)P₂ synthesis for membrane remodeling during dorsal ruffle formation.

Results

The N-terminal region of SH3YL1 is an evolutionarily conserved and structurally independent domain with high affinity for phosphoinositides

While searching the Pfam database for proteins with an SH3 domain in their C termini, we identified an unexplored domain species, domain of unknown function (DUF) 500. By sequence alignment, we found that the DUF500 domain is part of a longer amino acid sequence that is conserved from yeast to mammals (Fig. S1 A). Notably, this homologous region exists not only in eukaryotes, such as fungi, plants, and vertebrates, but also in Gram-negative bacteria (see Discussion).

To determine whether this entire region forms an independent structure that extends from the DUF500 domain to the N terminus, we predicted the domain boundary by using the support vector machine (SVM) long method (Ebina et al., 2009). In the primary sequence of human SH3YL1 (Aoki et al., 2000), a putative linker region separating two structural domains was predicted to be Gln230–Glu265 with a peak probability at Pro242 (Fig. 1 A), suggesting that ~230 N-terminal residues form a structurally independent unit. A similar result was obtained using the DomCut server (Suyama and Ohara, 2003),

which predicted Pro246 as the most probable linker position (unpublished data). These predictions were supported by the results of proteolytic digestion experiments, wherein purified FLAG-SH3YL1 (full length) protein was incubated with limiting amounts of trypsin. The N-terminal region of SH3YL1, which was recognized by anti-FLAG, was cleaved to an ~25-kD fragment, slightly larger than FLAG-SH3YL1 SYLF (1–216) (Fig. 1 B). A faint band was also observed around ~16 kD (Fig. 1 B, asterisk), suggesting another very minor cleavage site. These results indicate that the C-terminal region extending from Glu217 acts as the primary domain linker that is accessible to trypsin. Based on these data and our findings from this study, we define this ~220-residue-long N-terminal region as a single domain module named “SYLF” domain on the basis of its representative members (SH3YL1, Ysc84p/Lsb4p, Lsb3p, and plant FYVE protein; Fig. S1 B).

The yeast SYLF protein Ysc84p/Lsb4p localizes to actin patches and plays an important role in endocytosis (Dewar et al., 2002). The conserved N-terminal region binds to and forms a bundle of F-actin in vitro (Robertson et al., 2009). We attempted to recapitulate this finding by using SH3YL1, but neither full-length SH3YL1 nor its SYLF domain bound to F-actin (Fig. S1 C). In contrast, the SYLF domains of the budding yeast proteins Ysc84p/Lsb4p and Lsb3p, as well as actinin-1 (ACTN1), which was used as a positive control, showed efficient F-actin binding (Fig. S1 C).

The failure of SH3YL1 to bind F-actin suggests that it is not an evolutionarily conserved biochemical property, at least in mammalian SYLF domains. In addition, in pull-down experiments using HeLa cell lysate and rat brain cytosolic fractions, no proteins bound to the SH3YL1 SYLF domain–GST fusion protein (unpublished data). These results prompted us to examine whether it binds to phospholipids like the BAR and F-BAR domains in the proteins containing C-terminal SH3 domains. As expected, full-length and truncated recombinant proteins containing the SH3YL1 SYLF domain bound well to liposomes that were composed of acidic phospholipids from brain extracts (brain liposomes; Fig. 1 C). In contrast, a deletion mutant that lacked the SYLF domain (ΔSYLF) had nearly no affinity for liposomes. These results demonstrate that the SYLF domain is essential and adequate for lipid binding. Moreover, yeast SYLF domains had high affinities for liposomes (Fig. 1 D), indicating that lipid binding is an evolutionarily conserved property of the eukaryotic SYLF domains.

Next, we assessed the lipid-binding specificity of the full-length protein and found that it bound to PI(3,4,5)P₃ with the highest affinity (Fig. 1 E). Other D5-phosphorylated phosphoinositides such as PI(3,5)P₂ and PI(4,5)P₂ were also preferred compared with other acidic phospholipids. Similar results were obtained with the SYLF domain–only construct (Fig. S2 A), confirming that this module binds to phosphoinositides.

An amphipathic α helix at the N terminus of the SYLF domain is necessary for lipid binding

We observed that the predicted α -helical sequence at the N terminus of the SYLF domain (residues 9–23) contained many

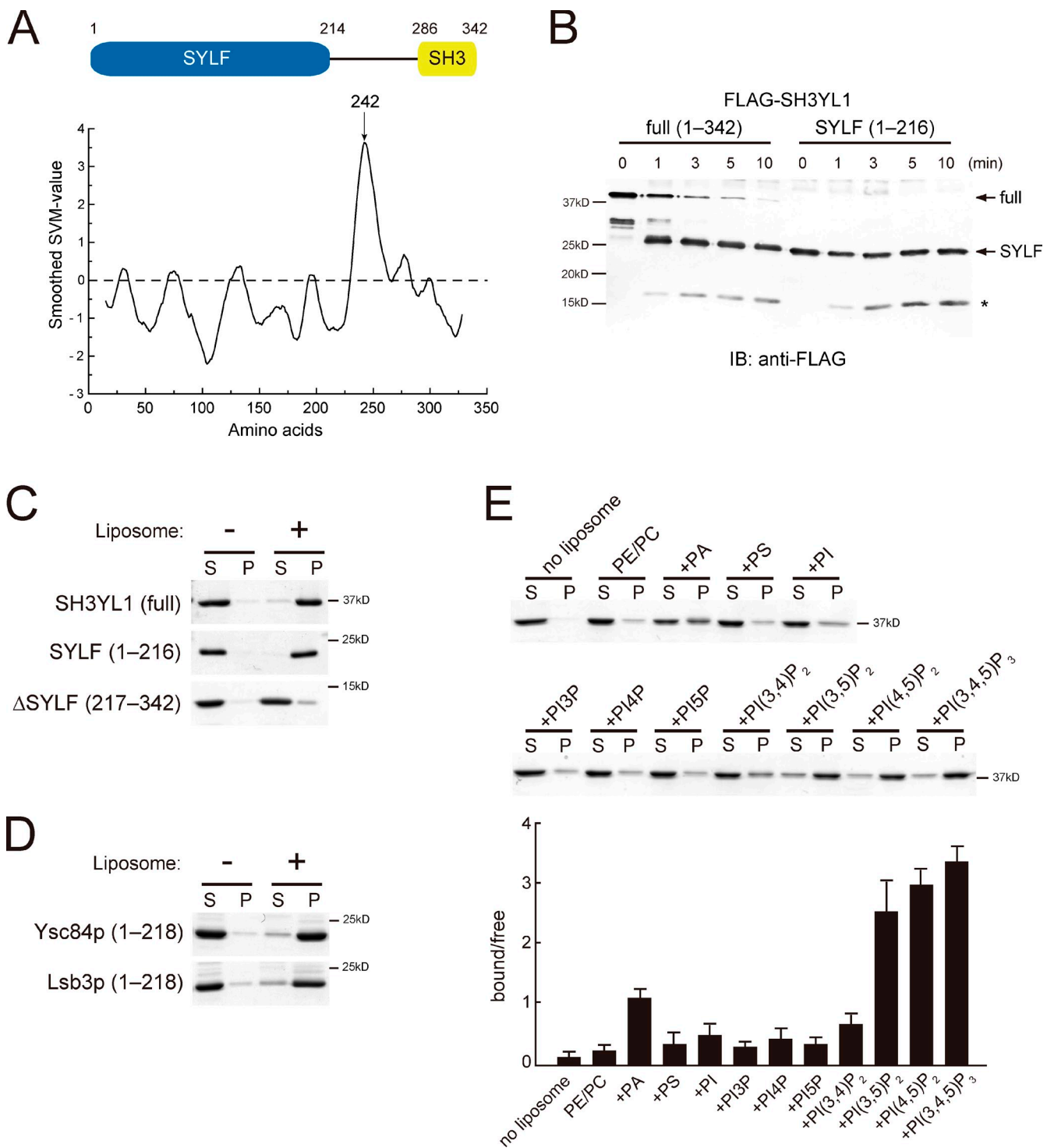


Figure 1. The N-terminal region of SH3YL1 with high affinity for phosphoinositides. (A) A schematic presentation of human SH3YL1 and domain linker prediction by the SVM long protocol. Smoothed SVM output values were plotted against the amino acid sequence. Larger values indicate higher probabilities of domain linkers. (B) Limiting proteolytic digestion. Purified FLAG-SH3YL1 (full length and SYLF) proteins were treated with trypsin for the indicated times and then immunoblotted (IB) with anti-FLAG antibodies. The asterisk shows a minor digestion product. (C) Liposome cosedimentation assay using brain liposomes and SH3YL1 (full length, SYLF, and Δ SYLF). Proteins in the supernatant (S) and pellet (P) are visualized by CBB staining. (D) Liposome cosedimentation assay using brain liposomes and Ysc84p and Lsb3p (1–218). (E) PE/PC-based liposomes supplemented with 10% of the indicated lipids were used in the cosedimentation assay and quantitative representation. Results are a mean (SD) of three independent experiments.

positively charged residues (Fig. 2 A). Moreover, this region was predicted to possess amphipathic properties (Fig. 2 B), suggesting that it plays an important role in lipid binding. To test this hypothesis, a deletion mutant ($\Delta 1-29$) was constructed and

subjected to lipid-binding assay. The deletion mutant ($\Delta 1-29$) showed much lower affinity than the full-length protein (Fig. 2 C), indicating the importance of this region. The contribution of the positively charged residues on the hydrophilic surface of

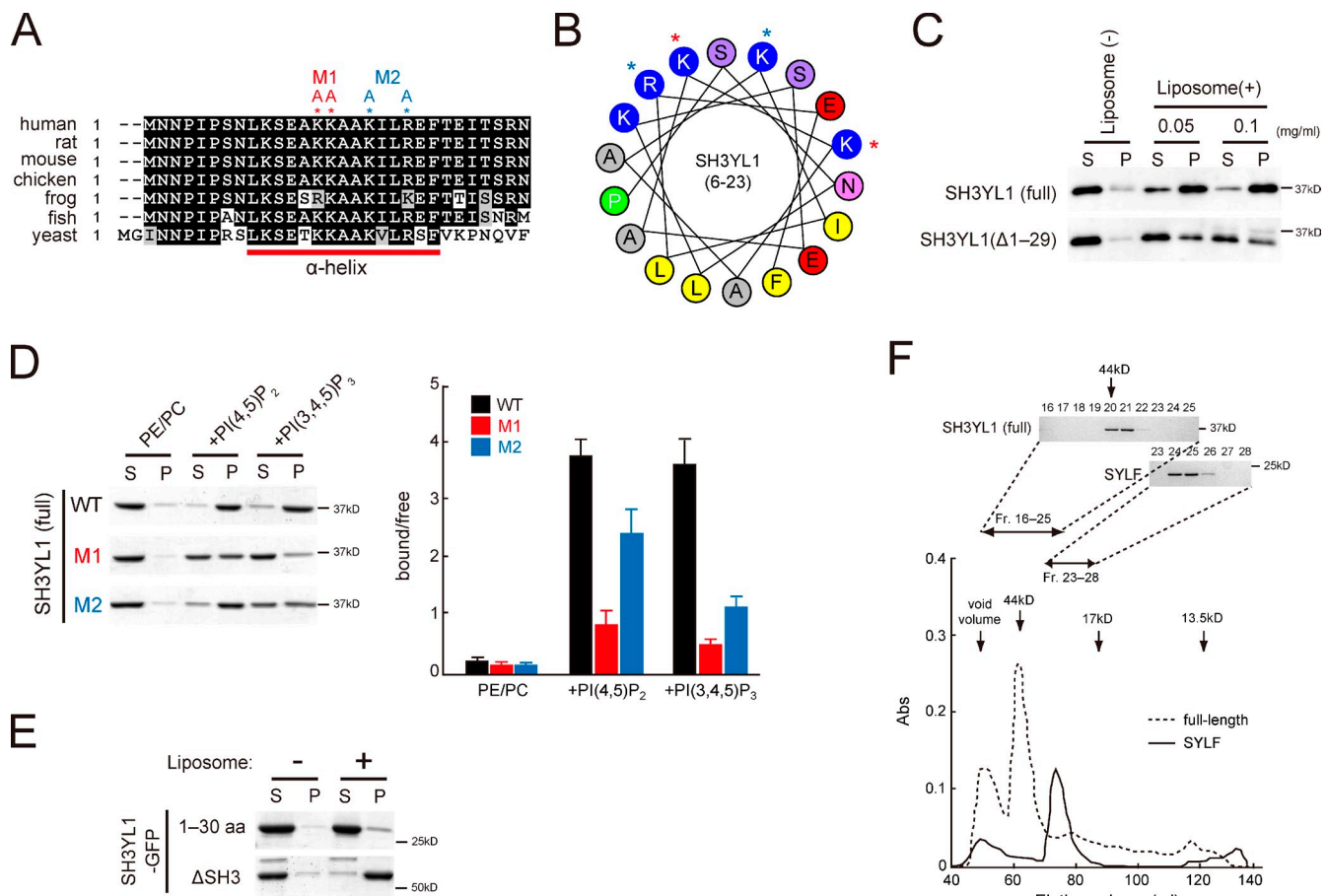


Figure 2. An amphipathic α helix at the N terminus of the SYLF domain is necessary for lipid binding. (A) Multiple sequence alignment of N-terminal regions of the SYLF domain from various species. The predicted α helix is indicated by a red line (residues 9–23), and mutated, positively charged residues in M1 and M2 are shown by asterisks. Identical amino acids are shaded in black, and similar residues are in gray. (B) A helical wheel representation of the SH3YL1 N-terminal region. Yellow, hydrophobic residues; purple, serine; blue, basic; pink, asparagine; red, glutamic acid; green, proline; and gray, other residues. Mutated residues are shown by asterisks. (C) Liposome cosedimentation assay using full-length or Δ 1–29 SH3YL1 mutant and brain liposomes. Proteins are visualized by immunoblotting with anti-SH3YL1 antibodies. (D) PE/PC-based liposomes supplemented with 10% of PI(4,5)P₂ or PI(3,4,5)P₃ were used in the cosedimentation assay and quantitative representation. WT, wild type. Results are a mean (SD) of three independent experiments. (E) Liposome cosedimentation assay using 1–30 or Δ SH3 SH3YL1-GFP mutant and brain liposomes. Proteins are visualized by CBB staining. (F) Gel filtration chromatography of SH3YL1 (full length and SYLF). Eluted fractions were measured at 280 nm and then visualized by CBB staining. Abs, absorbance.

this region (Lys14 + Lys15 [M1] or Lys18 + Arg21 [M2]) was determined by replacing them with alanine (Fig. 2, A and B). In comparison with wild type, the binding affinity of these mutants for PI(3,4,5)P₃, especially that of the M1 mutant, was significantly low (Fig. 2 D).

Notably, the 30 residues of the N terminus (1–30) bound poorly to the brain liposomes (Fig. 2 E), indicating that this α helix alone is inadequate for binding and that the remainder of the region makes a significant contribution to the lipid binding. This phenomenon was not attributed to the avidity generated as a result of apparent dimerization or oligomerization through the remainder of the region because the full-length SH3YL1 and SYLF domain are monomeric, as shown by gel filtration (Fig. 2 F). Together with the fact that the Δ 1–29 mutant still retains \sim 40% of binding (Fig. 2 C), these data collectively suggest that the SYLF domain has a lipid-binding surface, which is formed by positively charged residues in the N-terminal amphipathic helix and unidentified residues in the remainder of the domain.

SH3YL1 localizes to the plasma membrane at an early stage of dorsal ruffle formation

Growth factor stimulation induces the dynamic and transient formation of membrane ruffles on the dorsal surface of NIH3T3 cells (Mellström et al., 1988; Buccione et al., 2004). Because SH3YL1 strongly bound to PI(3,4,5)P₃, which is produced by growth factor stimulation, we investigated whether SH3YL1 localizes to the PDGF-induced dorsal ruffles.

Under serum-starved conditions (0 min), HA-tagged SH3YL1 (HA-SH3YL1) was localized to the cytosol in NIH3T3 cells. 2 min after PDGF stimulation, HA-SH3YL1 was recruited to a plasma membrane structure with short actin filaments that were aligned in a circular pattern (Fig. 3 A). This structure appeared to be an immature form of dorsal ruffles, suggesting that SH3YL1 functions at an early stage of dorsal ruffle formation. At 5 min, HA-SH3YL1 accumulated at mature and circular dorsal ruffles that were rich in dense F-actin structures. Consistent with the observations in previous studies (Araki et al., 1996; Suetsugu et al., 2003), dorsal ruffle formation was

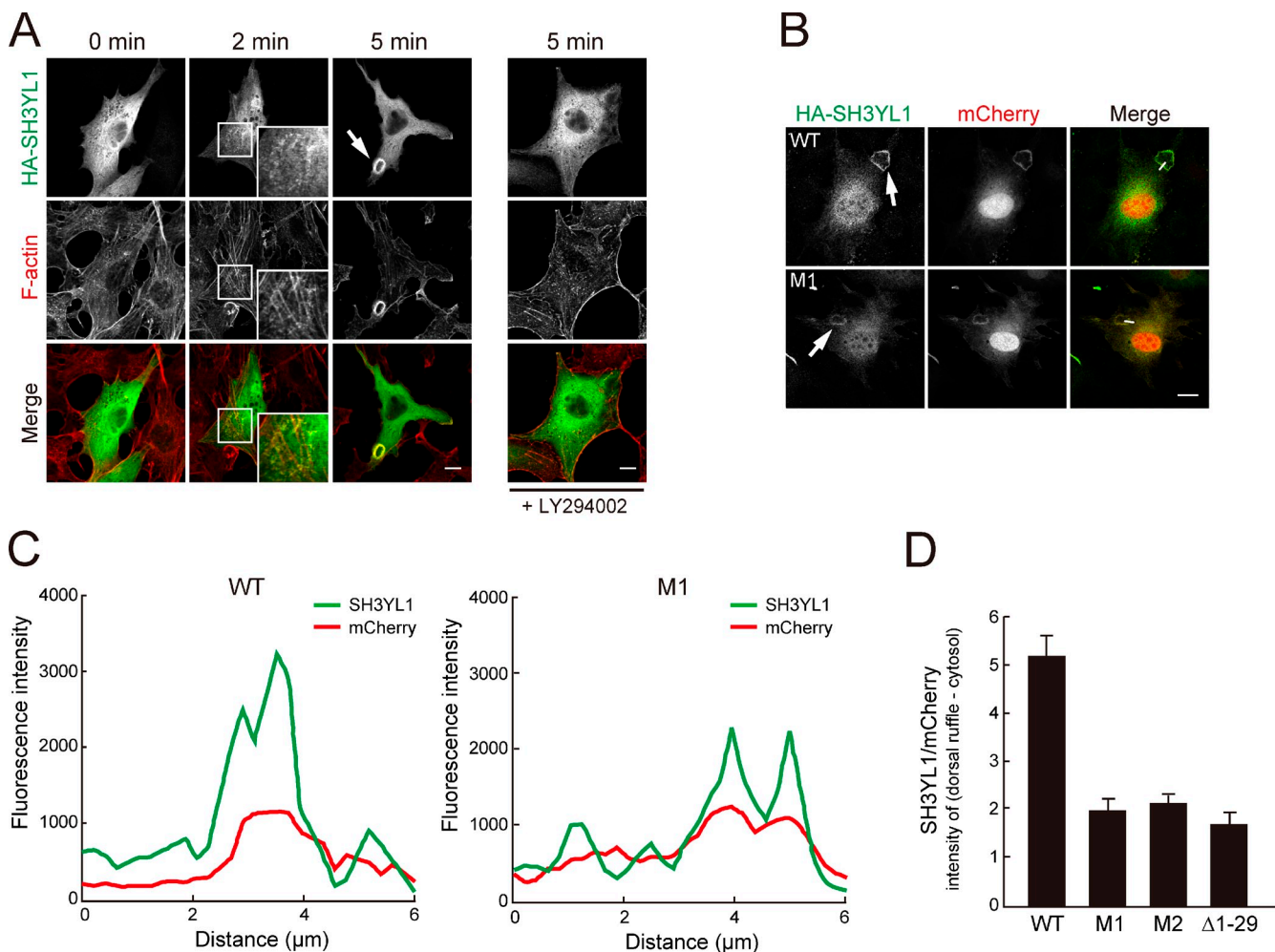


Figure 3. Localization of SH3YL1 at the dorsal ruffle. (A) NIH3T3 cells expressing HA-SH3YL1 (full length) were stimulated with 20 ng/ml PDGF for the indicated times and stained with anti-HA antibodies and rhodamine-phalloidin. Insets, precursor structures at a high magnification. Where indicated, 25 μM LY294002 was applied for 30 min before stimulation. (B) Localization of wild-type (WT) HA-SH3YL1 and mutant (M1) at 5 min after PDGF stimulation. (A and B) Arrows, circular dorsal ruffles. Bars, 10 μm . (C) Fluorescence intensity profiles of white lines in B. (D) Fluorescence intensities in the cytosol were subtracted from those at circular dorsal ruffles. The ratio of anti-HA versus mCherry are presented. Results are a mean (SD) of four experiments.

blocked by LY294002, a PI3K inhibitor (Fig. 3 A), indicating that D3-phosphorylated phosphoinositides and their binding partners are involved in this process.

Next, we studied whether the lipid-binding activity of SH3YL1 is required for its localization to the dorsal ruffles. The SYLF domain, which was determined to be essential for phosphoinositide binding, was sufficient for localization to the dorsal ruffles (Fig. S2 B). In addition, the density of the mutant form of SH3YL1, which has reduced affinity for phosphoinositides (Fig. 2 D, HA-SH3YL1 [M1]), was lower at the dorsal ruffles (Fig. 3, B and C) compared with that of the wild type. To quantify these findings, we measured the fluorescence intensities of HA-SH3YL1 as well as mCherry protein, which was coexpressed as a cytosolic marker of the dorsal ruffle area, to calculate the net intensity by subtracting the cytosolic signal. As shown in Fig. 3 D, the localization of the M1, M2, and $\Delta 1-29$ mutants to the dorsal ruffles was significantly lower than that observed in the case of wild type, demonstrating that SH3YL1 is recruited to the plasma membrane via PI3K-dependent SYLF-phosphoinositide interactions.

SH3YL1 is necessary for dorsal ruffle formation

Because SH3YL1 localized to the dorsal ruffles, we assessed whether it was necessary for the formation of dorsal ruffles. Transfection of SH3YL1-targeting siRNAs resulted in the depletion of >90% of SH3YL1 protein but did not alter actin levels (Fig. 4 A). Dorsal ruffles were formed in ~60% of control siRNA-treated cells after PDGF stimulation, whereas significantly fewer ruffles were formed in SH3YL1 siRNA-treated cells (Fig. 4, B and C). This suppression was alleviated by the exogenous wild-type SH3YL1 but not by $\Delta 1-29$, M1, or M2 constructs (Fig. 4 C), suggesting that the presence of both the SH3 domain and a functional SYLF domain is necessary.

Dorsal ruffles have been implicated in macropinocytosis, which can be monitored with markers for fluid-phase endocytosis. Consistent with the dynamic association of SH3YL1 with dorsal ruffles, PDGF-dependent fluid-phase endocytosis was inhibited in SH3YL1 knockdown cells relative to control cells, as observed by dextran internalization assay (Fig. 4 D). To quantify this effect, we measured the uptake of HRP, a

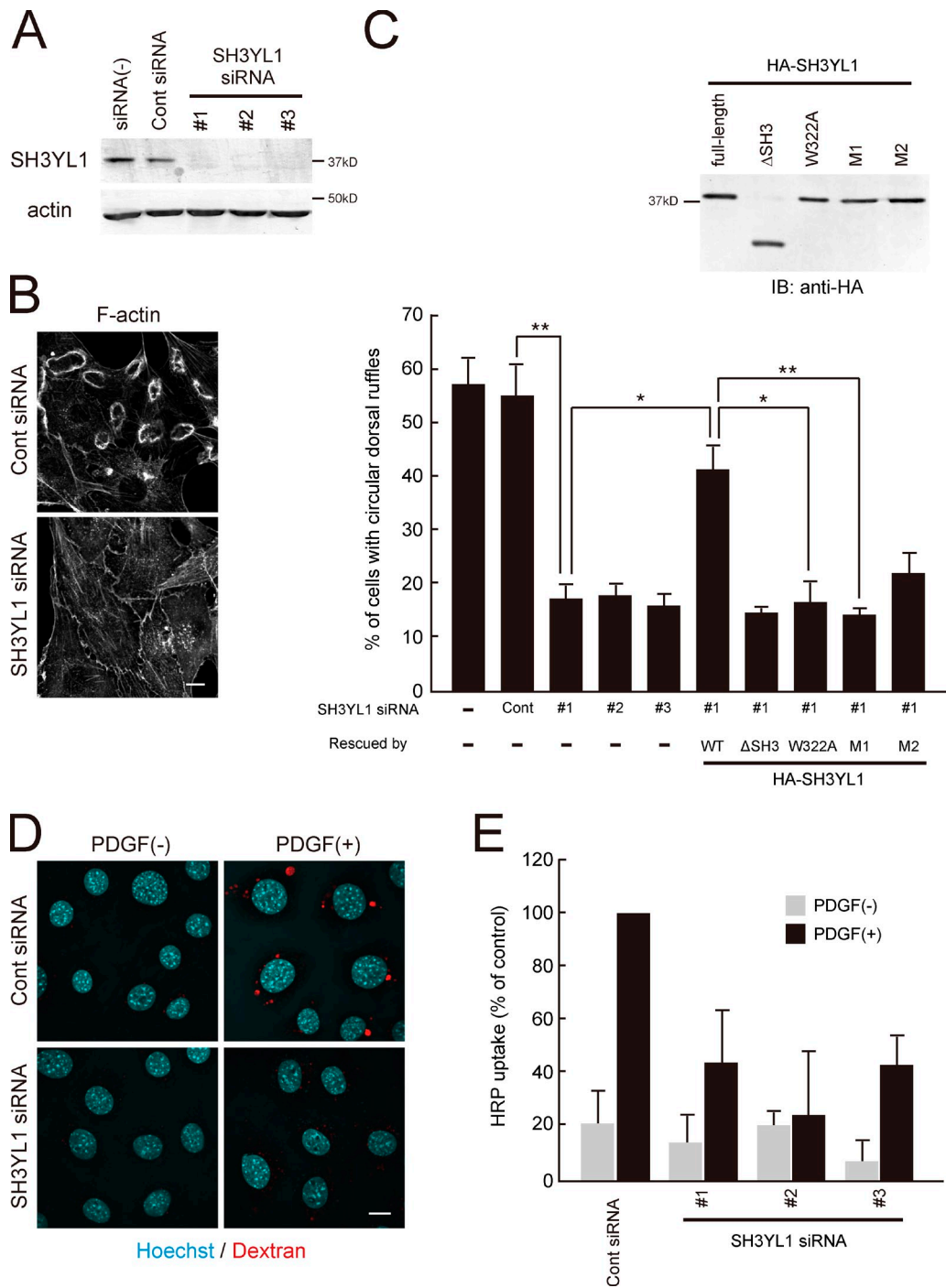


Figure 4. SH3YL1 is necessary for dorsal ruffle formation. (A) Anti-SH3YL1 immunoblots of NIH3T3 cells transfected with control or SH3YL1-specific siRNA. (B) Phalloidin staining of control or SH3YL1-depleted NIH3T3 cells treated with PDGF for 5 min. Bar, 10 μ m. (C) Percentages of cells generating at least one circular dorsal ruffle. Rescue experiments were performed by transfecting HA-SH3YL1 constructs (blot, expression levels of the indicated constructs) to recover circular dorsal ruffle formation. Results are a mean (SD) of three independent experiments; 200 cells counted (100 cells for the rescue experiments) per experiment. **, $P < 0.01$; *, $P < 0.05$. (D) Control or SH3YL1-depleted NIH3T3 cells were allowed to internalize the fluid-phase marker rhodamine-dextran (0.2 mg/ml; shown in red) for 10 min and then stained with Hoechst (cyan). Bar, 10 μ m. (E) NIH3T3 cells transfected with indicated siRNAs were subjected to HRP uptake assay for 10 min with or without PDGF stimulation (20 ng/ml). Results are a mean (SD) of three independent experiments.

marker of fluid-phase endocytosis. Knockdown of SH3YL1 expression by all three siRNAs resulted in a significant reduction in the PDGF-induced internalization of HRP (Fig. 4 E). These data demonstrate that the SH3YL1–phosphoinositide interaction regulates PDGF-induced dorsal ruffle formation and macropinocytosis.

SH3YL1 forms a complex with SHIP2, a phosphoinositide 5-phosphatase

To determine the molecular mechanism by which SH3YL1 mediates dorsal ruffle formation, we attempted to identify its binding proteins. The SH3 domain of SH3YL1 was expressed as a GST fusion protein and was used in a pull-down assay with

HeLa cell lysates. Several proteins were identified, including N-WASP and dynamin 2, which are typical binding partners for SH3 domains (Fig. 5 A).

Notably, SHIP2, a PI(3,4,5)P₃ 5-phosphatase that generates PI(3,4)P₂, was also identified in the pull-down fraction (Fig. 5 A). We decided to focus on this interaction because of its potential relevance to SH3YL1 function in PI3K-dependent dorsal ruffle formation. This interaction was reproduced using exogenous Myc-tagged SHIP2 (Myc-SHIP2), which was pulled down by GST-SH3 and GST-SH3YL1 (full length) but not by GST (Fig. 5 B). Moreover, SH3YL1 and SHIP2 interacted with each other in the HeLa cells that were transfected with FLAG-tagged SH3YL1 (FLAG-SH3YL1). As shown in Fig. 5 C, endogenous SHIP2 was detected in anti-FLAG immunoprecipitates from the lysates of FLAG-SH3YL1 (full length)-transfected cells but not from lysates of cells that were transfected with ΔSH3 or W322A, wherein a highly conserved tryptophan residue in the SH3 domain was mutated; this suggested that SH3YL1 interacts with SHIP2 through its SH3 domain. The W322A mutant was unable to rescue the impaired dorsal ruffle formation in SH3YL1 knockdown NIH3T3 cells (Fig. 4 C). Endogenous SHIP2 was detected in the anti-SH3YL1 immunoprecipitates from NIH3T3 cell lysates, further indicating that they form a complex *in vivo* (Fig. 5 D). We also determined this interaction to be direct, as shown in pull-down experiments using purified FLAG-SHIP2 (Fig. 5 E).

The C-terminal region of SHIP2 is rich in proline residues and mediates several interactions with SH3 domain-containing proteins (Fig. 5 F; Dyson et al., 2001; Xie et al., 2008). To our surprise, the deletion of a C-terminal region, including the proline-rich area (SHIP2 (1–740)), did not alter the coimmunoprecipitation of SHIP2 with SH3YL1 (Fig. 5 G). Conversely, deletion of the SH2 domain and a flanking region that is on the N-terminal side of the lipid phosphatase domain (SHIP2 (415–1,258)) nearly abolished the binding. In this flanking region, we identified an amino acid sequence, PPLPPR, that matched the class II consensus motif of SH3 domain-binding peptide (Mayer and Gupta, 1998; Kang et al., 2000). Indeed, the deletion (SHIP2 (Δ139–144)) and mutation (SHIP2 (PL140,141AA)) of this sequence resulted in loss of binding (Fig. 5 G).

We also examined whether the interaction between SH3YL1 and SHIP2 was regulated by growth factor stimulation. FLAG-SH3YL1-expressing NIH3T3 cells were treated with PDGF followed by immunoprecipitation with anti-FLAG. Compared with serum-starved conditions (0 min), the interaction significantly increased 5 min after PDGF treatment (Fig. 5 H). These results demonstrate that SH3YL1 and SHIP2 form a molecular complex through an interaction between the N-terminal proline-rich sequence in SHIP2 and the C-terminal SH3 domain of SH3YL1 that is regulated by PDGF.

SHIP2 is required for circular dorsal ruffle formation

To determine the function of SHIP2 in dorsal ruffle formation, NIH3T3 cells were transfected with Myc-SHIP2 and HA-SH3YL1 and stimulated with PDGF. As a result, significant colocalization of SH3YL1 and SHIP2 was observed at the circular dorsal ruffles (Fig. 6 A).

The function of SHIP2 was further examined in knockdown experiments (Fig. 6 B). In SHIP2 knockdown cells, the formation of ring-shaped circular dorsal ruffles was impaired, whereas the ruffles in the peripheral membrane remained intact (Fig. 6, C [arrow] and D). Notably, several relatively straight ruffles were formed at the dorsal plasma membrane, to which SH3YL1 also localized (Fig. 6, C [arrowheads], D, and E [arrows]). These effects were specifically suppressed by exogenous SHIP2, depending on its interaction with SH3YL1 (Fig. 6 D). The straight ruffles that were induced by SHIP2 knockdown are possibly malformed dorsal ruffles that cannot develop ring-shaped structures. Correspondingly, dextran uptake was also inhibited in SHIP2-depleted cells (Fig. 6 F). These data imply that SHIP2 functions with SH3YL1 and that SHIP2 mediates the formation of the circular membrane structure.

As shown in Fig. 5 A, our pull-down experiment also identified PI3K-C2β as a binding partner for the SH3 domain of SH3YL1. We confirmed this interaction of FLAG-SH3YL1 and endogenous PI3K-C2β (Fig. S3 A). Myc-tagged PI3K-C2β localized to the dorsal ruffles, and its suppression, as mediated by expression knockdown, inhibited dorsal ruffle formation (Fig. S3, B [top row], C, and E), indicating its importance.

SH3YL1 and SHIP2 are required for the production of PI(3,4)P₂, whose downstream target is necessary for circular dorsal ruffle formation

The preferred substrate for SHIP2 is PI(3,4,5)P₃, which generates PI(3,4)P₂ (Ishihara et al., 1999). To investigate the relationship between PI(3,4)P₂ levels and dorsal ruffle formation, we measured cellular levels of phosphoinositides after stimulation with PDGF by dot-blot assay. Production of PI(3,4,5)P₃ increased 2 min after stimulation with PDGF, when the dorsal ruffles were scarce (Fig. 7, A and B; and Fig. S5 A). In contrast, the generation of PI(3,4)P₂ was delayed compared with PI(3,4,5)P₃ and peaked 5 min after stimulation, when the formation of circular dorsal ruffles was nearly complete (Fig. 7, A and B). This result implies a link between PI(3,4)P₂ production and circular dorsal ruffle formation.

PI(3,4)P₂ production was significantly inhibited in SH3YL1- or SHIP2 siRNA-treated cells (Figs. 7 A [middle] and S5 A). In SH3YL1 knockdown cells, PI(3,4,5)P₃ synthesis was also reduced (Figs. 7 A [top] and S5 A). Considering the involvement of SH3YL1 and SHIP2 in dorsal ruffle formation (Figs. 4, B and C; and 6, C and D), these results strongly suggest that PI(3,4)P₂ is a prerequisite for this process.

Consistent with a previous study (Hogan et al., 2004), overexpression of Tapp1 pleckstrin homology (PH) domain, which possibly blocks endogenous PI(3,4)P₂-binding proteins in a competitive manner, suppressed dorsal ruffle formation (Fig. 7 C). Knockdown of endogenous Tapp1 also suppressed dorsal ruffle formation (Fig. S3, D and E), suggesting that Tapp1 is a downstream target of PI(3,4)P₂, which is required in this process. In support of this model, we observed that the exogenous HA-Tapp1 localized to the circular dorsal ruffles (Fig. S3 B, bottom row).

Overexpression of Grp1PH also inhibited dorsal ruffle formation (Fig. 7 C), implying that PI(3,4,5)P₃ is necessary.

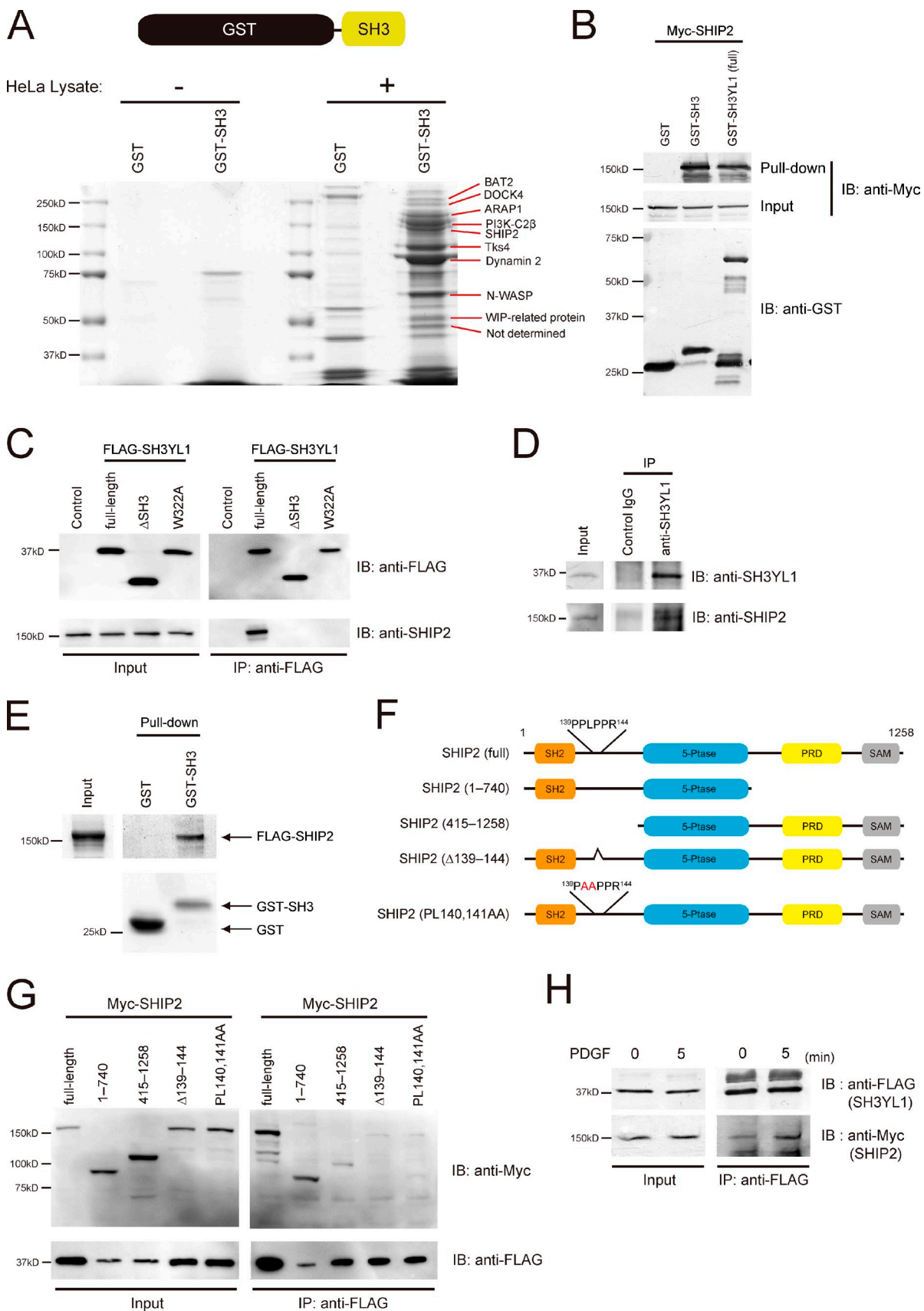


Figure 5. SH3YL1 forms a complex with SHIP2. (A) The GST or GST-SH3 domain of SH3YL1 was incubated with (+) or without (-) HeLa cell lysates. Bound fractions were visualized by CBB staining. Proteins identified by mass spectrometry are shown. (B) Lysates of COS-1 cells expressing Myc-SHIP2 were pulled down by GST, GST fusions with the SH3 domain, or full-length SH3YL1 and then immunoblotted with anti-Myc or anti-GST antibodies. (C) FLAG-SH3YL1 (full

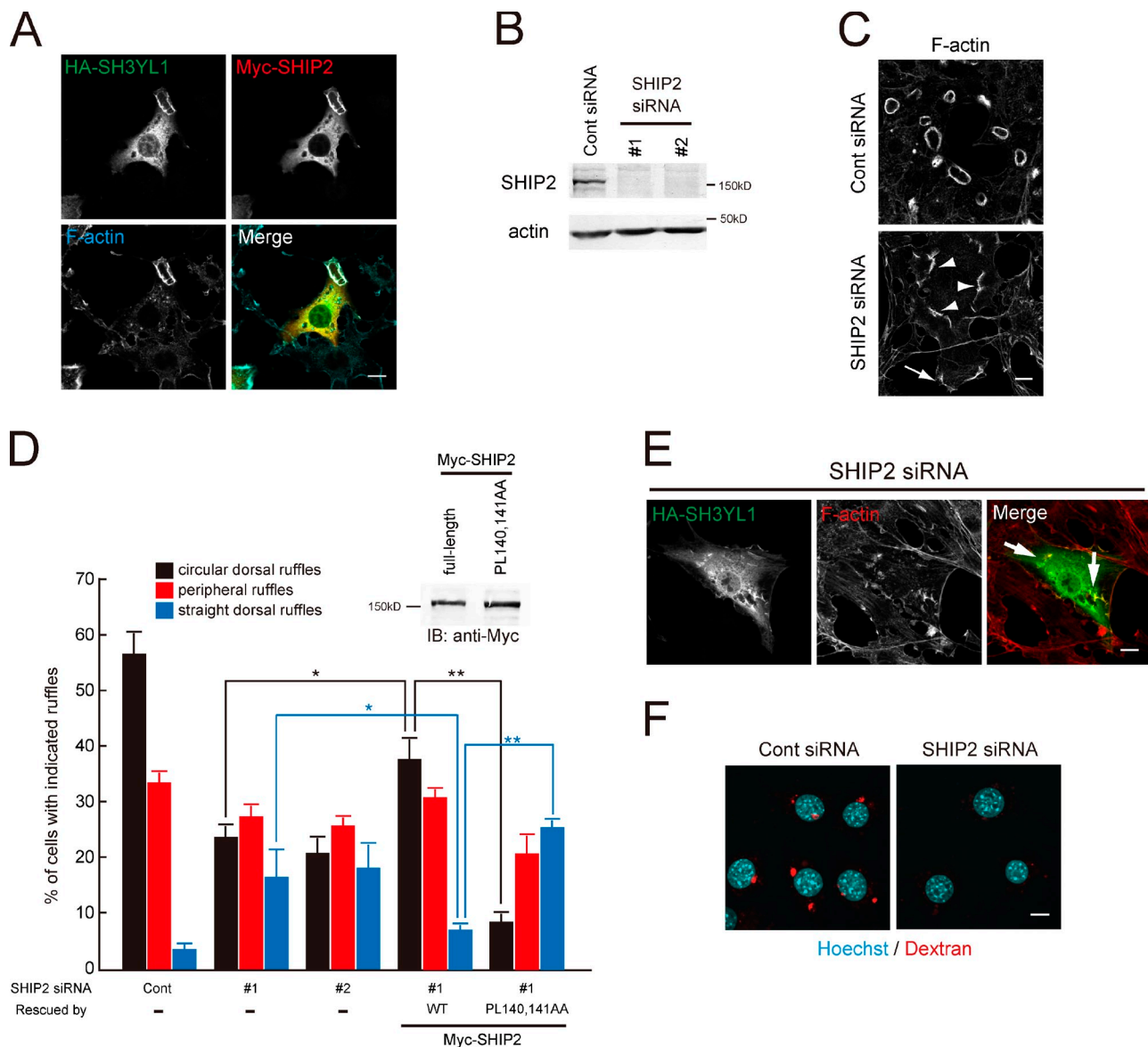
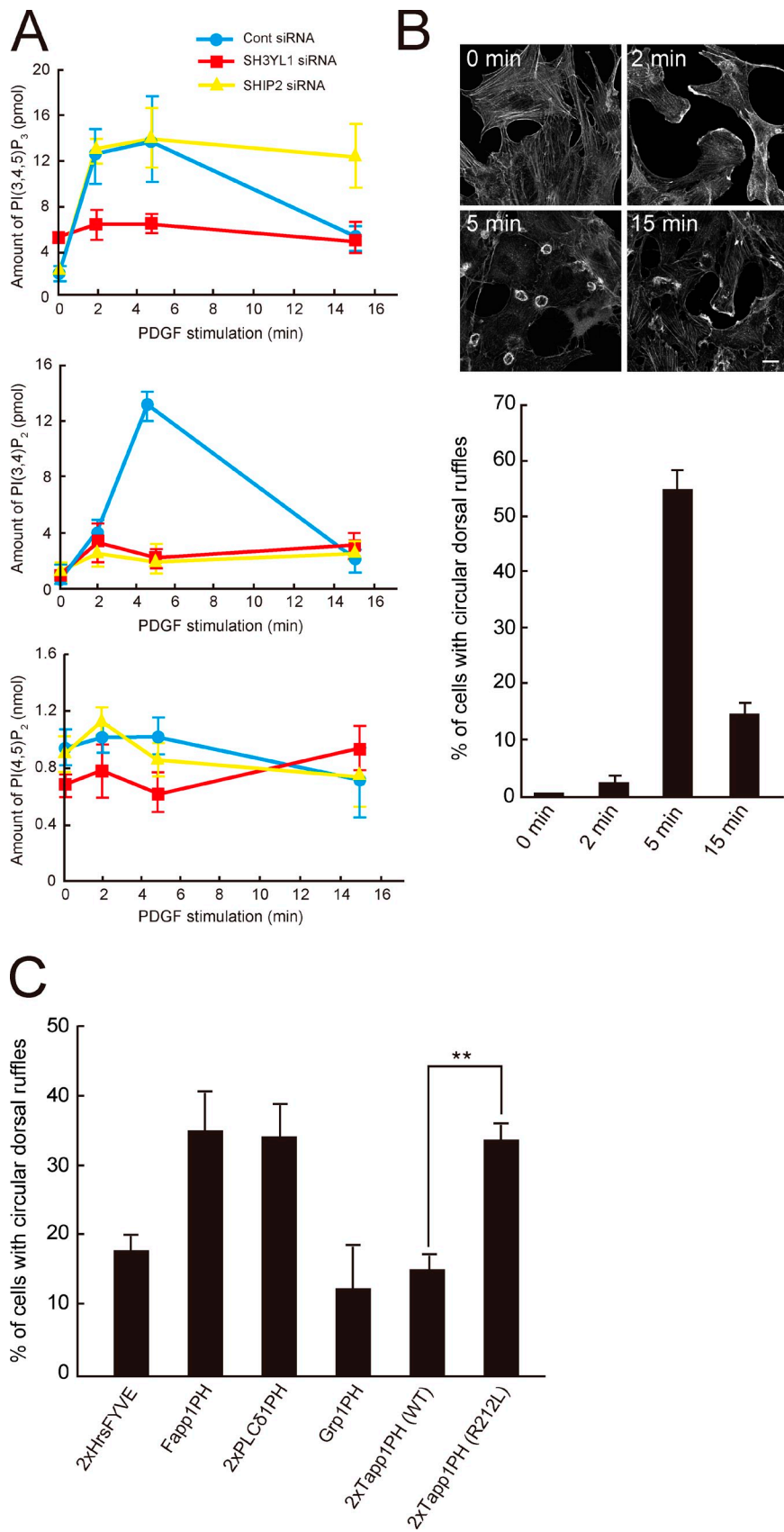


Figure 6. SHIP2 is required for circular dorsal ruffle formation. (A) NIH3T3 cells transiently transfected with HA-SH3YL1 and Myc-SHIP2 were serum starved, stimulated with 20 ng/ml PDGF for 5 min, fixed, and stained with anti-HA, anti-Myc antibodies, and Alexa Fluor 647-phalloidin. Bar, 10 μ m. (B) Anti-SHIP2 immunoblot of NIH3T3 cells transfected with control or SHIP2-specific siRNA. (C) PDGF-induced circular dorsal ruffle formation was reduced in SHIP2-depleted NIH3T3 cells. Phalloidin staining of cells treated with control or SHIP2 siRNAs is shown. The arrow indicates peripheral ruffles, and arrowheads indicate straight dorsal ruffles. Bar, 10 μ m. (D) Percentages of cells generating at least one circular dorsal ruffle, peripheral ruffle, or straight dorsal ruffle. Rescue experiments were performed by transfecting Myc-SHIP2 constructs (blot, expression levels of the indicated constructs) to recover each ruffle formation. WT, wild type. Results are a mean (SD) of three independent experiments; 200 cells counted (100 cells for the rescue experiments) per experiment. **, $P < 0.01$ and *, $P < 0.05$. (E) SHIP2-depleted NIH3T3 cells transiently transfected with HA-SH3YL1 were serum starved, stimulated with 20 ng/ml PDGF for 5 min, fixed, and stained with anti-HA antibodies and rhodamine-phalloidin. Arrows indicate straight dorsal ruffles. Bar, 10 μ m. (F) Rhodamine-dextran (red) and Hoechst (cyan) images of NIH3T3 cells treated with SHIP2 or control siRNA and incubated for 10 min with 0.2 mg/ml rhodamine-dextran. Bar, 10 μ m.

length, Δ SH3, or W322A) expressed in HeLa cells was immunoprecipitated with anti-FLAG antibodies and immunoblotted with anti-FLAG or anti-SHIP2 antibodies. (D) Endogenous SH3YL1 was immunoprecipitated with anti-SH3YL1 antibodies using lysates of NIH3T3 cells and immunoblotted with anti-SH3YL1 or anti-SHIP2 antibodies. (E) Purified FLAG-SHIP2 was pulled down by GST and GST fusions with the SH3 domain and then visualized by CBB staining. (F) A schematic presentation of SHIP2 deletion and point mutants used in this study. The red text indicates introduced alanines instead of intact amino acids (proline and leucine). PRD, proline-rich domain; SAM, sterile α motif. (G) FLAG-SH3YL1 (full length) and the indicated Myc-SHIP2 mutants expressed in COS-1 cells were immunoprecipitated with anti-FLAG antibodies and immunoblotted with anti-FLAG or anti-Myc antibodies. (H) NIH3T3 cells transiently transfected with FLAG-SH3YL1 and Myc-SHIP2 were serum starved and then stimulated with 20 ng/ml PDGF for 0 and 5 min. Cells were harvested, and the lysate was immunoprecipitated with anti-FLAG antibodies and immunoblotted with anti-FLAG or anti-Myc antibodies.

Figure 7. Correlation between PI(3,4)P₂ synthesis and circular dorsal ruffle formation. (A) Lipids were extracted from control, SH3YL1-, or SHIP2-depleted NIH3T3 stimulated with 20 ng/ml PDGF for 0, 2, 5, and 15 min. Amounts of PI(3,4)P₂, PI(4,5)P₂, and PI(3,4,5)P₃ were quantified by Qdot-705-Tapp1-2xPH, Qdot-655-PLCδ1-PH, and Qdot-585-Grp1-PH, respectively, in the dot-blot assay. Data are a mean (SD) of three independent experiments. (B) Time course of circular dorsal ruffle formation. Phalloidin staining and quantifications are shown. Results are a mean (SD) of three independent experiments; 200 cells counted per experiment. Bar, 10 μ m. (C) Quantification of circular dorsal ruffles in NIH3T3 cells overexpressing lipid-binding domains. Percentages of cells with at least one circular dorsal ruffle are shown. Results are a mean (SD) of three independent experiments; 100 cells counted per experiment. **, $P < 0.01$.



We noted that overexpression of the Hrs FYVE domain also suppressed dorsal ruffle formation (Fig. 7 C), suggesting that endosomal trafficking is involved.

Dynamics of PI(3,4)P₂ formation and circular dorsal ruffle formation

To examine the molecular dynamics of circular dorsal ruffle formation, the distribution of F-actin, PI(3,4)P₂, SH3YL1, and SHIP2 was monitored in PDGF-stimulated NIH3T3 cells that were transfected with Lifeact-mCherry, a probe for F-actin (Riedl et al., 2008), by time-lapse microscopy. Consistent with the data shown in Fig. 3 A, numerous short F-actin filaments, which appeared to be dorsal ruffle precursors, were observed 3–4 min after stimulation followed by the formation of an F-actin-enriched circular structure at 6 min (Fig. 8 A).

The localization of SH3YL1, SHIP2, and PI(3,4)P₂ was determined in fixed cells. PI(3,4)P₂, which was visualized using Tapp1PH, localized specifically to the mature circular dorsal ruffles at 5 min but was not associated with precursor ruffles at 3 min (Fig. 8 B). In contrast, SH3YL1 and SHIP2 appeared at the precursor structure as early as 3 min, remaining at the mature dorsal ruffles (Fig. 8, B and C). These results suggest that SH3YL1 and SHIP2 are first recruited to the PI(3,4,5)P₃-enriched dorsal ruffle precursors, after which PI(3,4)P₂ is generated and the circular ruffles mature.

Time-lapse microscopy images of NIH3T3 cells expressing Lifeact-mCherry with SH3YL1-GFP or GFP-SHIP2 showed the recruitment of both proteins to the actin-enriched circular structures 3–4 min after PDGF treatment (Fig. S4, A and B). Similarly, PI(3,4,5)P₃ and PI(3,4)P₂ levels rose sequentially at circular dorsal ruffles (Fig. S4 C), indicating that phosphoinositide conversion took place.

Discussion

In this study, we identified the SYLF domain as a novel phosphoinositide-binding module. The SYLF domain also exists in the bacterial genome and is highly conserved in mammals and green plants (Fig. S1 B). The Pfam database and findings from our analysis using the SignalP and LipoP program (Juncker et al., 2003; Emanuelsson et al., 2007) revealed that bacterial proteins harboring the SYLF domain retain putative signal peptides at their N terminus and are thus likely to be exported to the periplasmic space or outer environment. The biochemical and physiological functions of SYLF proteins in the bacteria should be studied to learn about this newly identified lipid-binding module.

Conversely, eukaryotic SYLF domains have the lowest homologies to bacterial members, especially at the ~30 N-terminal residues, but they contain amphipathic α helices. Findings from our in silico and in vitro analyses support that the entire SYLF domain in human SH3YL1, including the amphipathic α helix, is an independent structure (Fig. 1, A and B). Moreover, we have implicated the positively charged residues (Lys14, Lys15, Lys18, and Arg21) in a putative amphipathic α helix in lipid binding (Fig. 2 D). Previous studies have demonstrated that some lipid-binding modules, such as the ENTH and N-terminal

amphipathic helix and BAR (N-BAR) domains, have N-terminal amphipathic α helices that mediate membrane curvature generation and/or sensing (Farsad et al., 2001; Ford et al., 2002; Bhatia et al., 2009). With regard to lipid-binding mechanisms, structural analyses of these domains have revealed a single binding pocket in the former and a relatively flat binding surface in the latter, to both of which the N-terminal α helices and the remainder of the region contribute equally (Ford et al., 2002; Gallop et al., 2006). The crystal structure of the SYLF domain will help determine the mechanism by which this novel lipid-binding module recognizes membrane lipids with its amphipathic α helix. We have not observed any curvature dependency in membrane binding by the SYLF domain of SH3YL1 (unpublished data). We are interested in determining whether the SYLF domain retains any membrane-deforming activity, as the ENTH and N-BAR domains have.

Ysc84p/Lsb4p, an SYLF protein in budding yeast, localizes to actin patches at the plasma membrane and binds directly to F-actin through its N-terminal region in vitro (Dewar et al., 2002; Robertson et al., 2009). On the basis of these findings, this region, which corresponds to the SYLF domain in mammals, was termed the Ysc84 actin-binding domain (Robertson et al., 2009). However, despite its significant homology to the Ysc84 actin-binding domain, the SYLF domain of SH3YL1 did not bind to F-actin (Fig. S1 C); instead, it bound to the phosphoinositides, including PI(3,4,5)P₃ (Fig. 1, C and E). The yeast SYLF domains of Ysc84p/Lsb4p and Lsb3p also bound robustly to brain liposomes composed of acidic phospholipids, including PI(4,5)P₂ (Fig. 1 D), indicating that this lipid-binding activity is highly conserved. Because PI(3,4,5)P₃ is believed to be absent in yeast, these SYLF proteins might be used for interactions with phosphoinositides in yeast, such as PI(3,5)P₂ and PI(4,5)P₂.

Using the SH3 domain of SH3YL1 as a probe, we identified several interacting partners, including the PI(3,4,5)P₃ 5-phosphatase SHIP2. Our results are consistent with the observation that the SYLF domain binds preferentially to PI(3,4,5)P₃. This model is supported by findings that the SH3 domain deletion mutant (Δ SH3) and the binding-incompetent mutant (W322A) of SH3YL1 were unable to rescue dorsal ruffle formation in the SH3YL1-depleted NIH3T3 cells (Fig. 4 C), suggesting that SHIP2 binding is critical for this process. Similarly, SH3YL1 binding is required for SHIP2 to recover circular dorsal ruffle formation in SHIP2 knockdown cells (Fig. 6 D). On the basis of our results, we propose the following model of dorsal ruffle formation: (a) upon stimulation by growth factors, SH3YL1 is recruited to the dorsal surface of the plasma membrane via interactions between its SYLF domain and PI(3,4,5)P₃; (b) SHIP2 is targeted to the SH3 domain of SH3YL1, where it dephosphorylates PI(3,4,5)P₃, generating PI(3,4)P₂; and (c) Tapp1 is recruited to the PI(3,4)P₂-enriched membrane site, promoting dorsal ruffle formation (Fig. 8 D).

The cellular localization and functions of PI(3,4)P₂ are poorly understood because it has been recognized only as a PI(3,4,5)P₃ metabolite. Recently, our group demonstrated that PI(3,4)P₂ is enriched in and is crucial for the formation of podosomes in Src-transformed NIH3T3 cells (Oikawa et al., 2008).

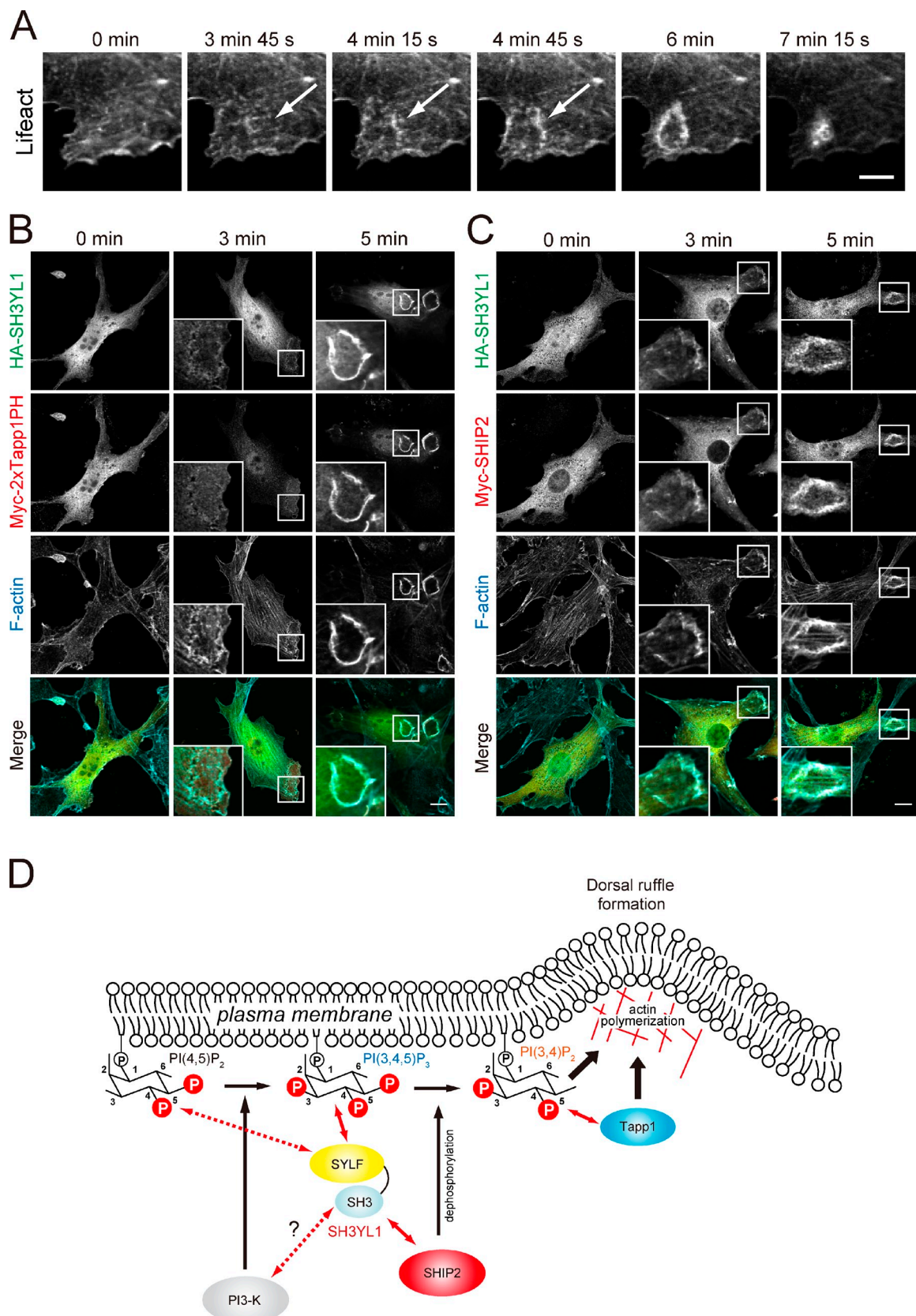


Figure 8. Dynamics of SH3YL1, SHIP2, and PI(3,4)P₂ at the circular dorsal ruffle. (A) Time-lapse images of F-actin probed by Lifeact-mCherry transfected in NIH3T3 cells stimulated with 20 ng/ml PDGF. Arrows indicate precursor structures. Bar, 10 μ m. (B and C) NIH3T3 cells transiently transfected with HA-SH3YL1 and Myc-2xTapp1PH (B) or HA-SH3YL1 and Myc-SHIP2 (C) were stimulated with 20 ng/ml PDGF for 3 and 5 min, fixed, and stained with anti-HA, anti-Myc antibodies, and Alexa Fluor 647-phalloidin. Bars, 10 μ m. Insets show the boxed areas at high magnification. (D) A model for circular dorsal ruffle formation by SH3YL1 and SHIP2. See Discussion for details.

The similarity in appearance between the dorsal ruffles and the podosomes, which are circular F-actin–enriched structures, implicates a common mechanism mediated by PI(3,4)P₂ and its downstream targets. However, the lipid phosphatases that generate PI(3,4)P₂ may differ between these cases, as SHIP2 is essential for dorsal ruffle formation but not for podosomes, which require synaptojanin 2 instead (Oikawa et al., 2008). A recent study has shown that accumulation of PI(3,4)P₂ by suppression of INPP4B results in enhanced Akt activation and tumorigenesis (Gewinner et al., 2009). Moreover, INPP4A, another PI(3,4)P₂ 4-phosphatase, mediates the suppression of glutamate excitotoxicity in the central nervous system (Sasaki et al., 2010). These studies and the present findings strongly suggest that PI(3,4)P₂ is not only a degradation product of PI(3,4,5)P₃, but it also has its own functions *in vivo*.

In addition to SHIP2, SH3YL1 interacted with several proteins such as PI3K-C2β, Tks4, and dynamin 2 through its SH3 domain. We showed that PI3K-C2β is important for the formation of dorsal ruffles (Fig. S3 E). PI3K-C2β phosphorylates phosphatidylinositol to generate PI(3)P *in vitro* (Sindić et al., 2001; Foster et al., 2003). In support of this, dorsal ruffle formation was blocked by overexpression of Hrs FYVE, which masks PI(3)P on early endosomes. Correspondingly, a recent study has shown that Rab5-mediated endocytosis is required for the activation of Rac on early endosomes to initiate the formation of dorsal circular ruffles (Palamidessi et al., 2008). PI3K-C2α, another isoform of the class II PI3K, alters its substrate specificity when it binds to clathrin in such a manner that facilitates PI(3,4,5)P₃ formation (Gaidarov et al., 2001). If this were also the case for PI3K-C2β when it binds to SH3YL1, it would explain the reduction in PI(3,4,5)P₃ formation after PDGF stimulation in SH3YL1 knockdown cells (Fig. 7 A). In support of this model, we have observed that PI(3,4,5)P₃ production decreases by PI3K-C2β knockdown (Fig. S5 B).

Depletion of Tks4 had minimal effects on dorsal ruffle formation (unpublished data). Tks4 is a scaffolding protein with an N-terminal phox homology domain, four SH3 domains, and several proline-rich motifs, which are required for the formation of the podosome, another circular F-actin structure rich in PI(3,4)P₂ (Oikawa et al., 2008; Buschman et al., 2009). Given that podosomes form at the ventral surface of the cell, Tks4 might function with SH3YL1 at the ventral, but not dorsal, side of the plasma membrane.

Dynamin 2 might also contribute to the regulation of the dorsal ruffles in complex with SH3YL1. Previous studies have indicated that dynamin 2 is recruited to the dorsal ruffles, and the expression of a dominant-negative form of dynamin 2 (K44A) strongly inhibits PDGF-induced macropinocytosis (Krueger et al., 2003; Schlunck et al., 2004). Consistent with the findings of a recent study (Liu et al., 2008), the suppression of dynamin 2 by RNAi resulted in the inhibition of dorsal ruffle formation (unpublished data). However, the mechanism underlying SH3YL1 functioning in conjunction with dynamin 2 remains to be determined.

In summary, we have identified a new class of lipid-binding modules, termed the SYLF domain, in SH3YL1. Our data

support a model in which the SH3YL1–SHIP2 complex promotes dorsal ruffle formation by conversion of PI(3,4,5)P₃ to PI(3,4)P₂. Future studies should determine molecular mechanisms by which the downstream targets of these phosphoinositides coordinate the circular array of the actin filaments in the dorsal ruffle.

Materials and methods

Reagents and antibodies

Mouse anti-HA monoclonal antibody and rabbit anti-Myc and anti-SHIP2 polyclonal antibodies were purchased from Cell Signaling Technology. Mouse anti-FLAG monoclonal antibody was purchased from Sigma-Aldrich. Mouse anti-PI3K-C2β monoclonal antibody was obtained from BD, and mouse anti-actin monoclonal antibody was obtained from Millipore. Rabbit anti-Tapp1 and anti-GST polyclonal antibodies were purchased from Santa Cruz Biotechnology, Inc. Anti-SH3YL1 polyclonal antibodies were raised by immunizing rabbits with recombinant SH3YL1 proteins (residues 217–342). All fluorescent reagents (rhodamine, Alexa Fluor 647–phalloidin, and Alexa Fluor 488– and 568–conjugated goat anti–rabbit or anti–mouse secondary antibodies) were purchased from Invitrogen. The bovine brain lipid extract used in the preparation of the brain liposome and phosphatidic acid were purchased from Sigma-Aldrich. Purified phospholipids (phosphatidylinositol, phosphatidylserine, phosphatidylethanolamine [PE], and phosphatidylcholine [PC]) were purchased from Avanti Polar Lipids, Inc. All phosphorylated phosphoinositides [PI(3)P, PI(4)P, PI(5)P, PI(3,4)P₂, PI(3,5)P₂, PI(4,5)P₂, and PI(3,4,5)P₃] were obtained from CellSignals Inc. Recombinant human PDGF-BB was obtained from Wako Chemicals USA. LY294002 and trypsin (from bovine pancreas) were purchased from Sigma-Aldrich.

Plasmids

IMAGE clone 3996066 (human SH3YL1) was purchased from Invitrogen, and then the full-length sequence was amplified with specific primers (5'-GCG-GATCCATGAAATACCTATAC-3' and 5'-GCGTCGACTTAATCATGGT-TACGTAGT-3') and subcloned into pGEX-6P-1 (GE Healthcare), pEGFP-N3 (Takara Bio Inc.), pCMV-HA, and pEF-BOS-FLAG vectors. SH3YL1 deletion and point mutants were amplified by PCR with specific primers and ligated into each vector. SH3YL1 deletion mutants (ΔSH3 and 1–30) were subcloned into pGEX-6P-3-GFP vector. The yeast Ysc84p (1–218) and Lsb3p (1–218) were amplified from *Saccharomyces cerevisiae* cDNA by PCR with specific primers (5'-GCGGATCCATGGGTATAATAATCCAAT-3' and 5'-GCGTCG-CAAAGTTGAACGCTTGTATT-3' for Ysc84p and 5'-GCGGATCCATGGG-TATAACAATCCTAT-3' and 5'-GCGTCGACGTAATAAACGCCCTGGACT-3' for Lsb3p) and subcloned into pGEX-6P-1 vector. Coding sequences of the human SHIP2 and PI3K-C2β were amplified from HeLa cDNA by PCR with specific primers (5'-GCGAATTCCACCATGGCCTCGGGCTGGGG-3' and 5'-GCGTCGACCTTGCTGAGCTGAGGGTGTCC-3' for SHIP2 and 5'-GCGAATTCCACCATGCTTCGACTCAGGACA-3' and 5'-GCGTCGAC-CAAGGTGCCATGACTTCGAGAT-3' for PI3K-C2β) and then subcloned into pCMV-Tag3B (Agilent Technologies) and pEGFP-C1 (Takara Bio Inc.) vectors. SHIP2 deletion and point mutants were amplified by PCR with specific primers and ligated into pCMV-Tag3B vector. Human 2xHrsFYVE, Fapp1PH, 2xPLC81PH, Grp1PH, 2xTapp1PH, and 2xTapp1PH (R212L; lipid-binding inactive form) cDNA fragments were subcloned into pCMV-HA, pCMV-Tag3B, and pTagRFP-C (Evrogen) vectors (Oikawa et al., 2008). Btk-PH-GFP construct was a gift from T. Sasaki (Akita University, Akita, Japan). The mCherry-lifeact construct was generated by Shusaku Kurisu (Kobe University Graduate School of Medicine, Kobe, Japan) as previously described (Riedl et al., 2008). Human Tapp1 cDNA was subcloned into pCMV-HA vector.

Protein expression and purification

Recombinant GST-fusion SH3YL1 (full-length, SYLF, ΔSYLF, and SH3 domain), Ysc84p (1–218), and Lsb3p (1–218) proteins were expressed in BL21 bacterial strain and then purified with glutathione Sepharose 4B (GE Healthcare) according to the manufacturer's instruction. Removal of GST was performed by on-column cleavage with PreScission protease (GE Healthcare). Recombinant FLAG-tagged SH3YL1 (full length and SYLF) and SHIP2 proteins were expressed in FreeStyle 293-F cells (Invitrogen) using FreeStyle MAX reagent (Invitrogen) and then were purified with ANTI-FLAG M2-agarose (Sigma-Aldrich) according to the manufacturer's instruction.

Proteolytic digestion

1 μ g purified FLAG-SH3YL1 (full length and SYLF) proteins was digested in buffer (50 mM Tris, pH 7.5, 10 mM MgCl₂, 50 mM KCl, and 1 M urea) with 0.1 μ g trypsin for 1, 3, 5, and 10 min at RT. After each reaction was terminated by the addition of 4x sample buffer, the products were analyzed by SDS-PAGE and immunoblotting.

Gel filtration chromatography

Gel filtration chromatography was performed by using a Superdex 75 pg 26/60 column (GE Healthcare) connected with the AKTA prime plus system (GE Healthcare). Protein samples and Gel Filtration Standard (Bio-Rad Laboratories) were loaded onto the column equilibrated with a buffer (50 mM Hepes, pH 7.4, 150 mM NaCl, 1 mM EDTA, and 1 mM DTT).

Cell culture and transfection

HeLa and COS-1 cells were maintained in DME supplemented with 10% FBS, and NIH3T3 cells were maintained in DME supplemented with 10% calf serum. Transfection was performed using Lipofectamine 2000 (Invitrogen) for HeLa and COS-1 cells and using Lipofectamine LTX (Invitrogen) for NIH3T3 cells. Experiments were performed 24 h after transfection.

RNAi

For knockdown of SH3YL1, SHIP2, PI3K-C2 β , or Tapp1, validated siRNAs were purchased from Invitrogen. 50 nM siRNAs was transfected into NIH3T3 cells with Lipofectamine RNAiMAX (Invitrogen), and the expression levels were assessed after 72 h by Western blotting or RT-PCR.

Endocytosis assay

To analyze macropinocytosis, cells were starved in serum-free DME for 16 h and then incubated with 1 mg/ml HRP (Invitrogen) in DME \pm 20 ng/ml PDGF for 10 min at 37°C. The uptake was stopped by transferring to 4°C, and cells were washed five times with cold PBS with 1 mM MgCl₂ and 1 mM CaCl₂ and twice with cold PBS. Cells were lysed with PBS containing 0.5% Triton X-100, and aliquots were assayed for enzyme activity (absorbance at 490 nm) by using σ -phenylenediamine as a substrate and for protein concentration (absorbance at 595 nm) using the BCA Protein Assay kit (Thermo Fisher Scientific). For dextran uptake, cells were starved in serum-free medium for 16 h, incubated with 0.2 mg/ml tetramethylrhodamine-labeled lysine-fixable 10-kD dextran (Invitrogen) in DME \pm 20 ng/ml PDGF for 10 min at 37°C, and then were fixed and stained with Hoechst 34580 (Invitrogen) for immunofluorescence.

Immunoblotting and immunoprecipitation

Cells were washed twice with PBS and lysed with lysis buffer (25 mM Hepes, pH 7.5, 0.5% Triton X-100, 2 mM EDTA, and 100 mM NaCl) supplemented with 5 μ g/ml aprotinin, 1 μ g/ml leupeptin, and 1 mM PMSF. The cell lysates were precleared with immobilized protein A (Thermo Fisher Scientific) and then with FLAG-tagged proteins or SH3YL1 immunoprecipitated with ANTI-FLAG M2-agarose or anti-SH3YL1 antibody for 4 h at 4°C with rotation. Complexes were washed four times in lysis buffer. Immunoprecipitated proteins were analyzed by SDS-PAGE and immunoblotting.

GST pull-down assays

10 mg HeLa cell lysates was mixed with 50 μ g GST-SH3 proteins bound to glutathione Sepharose 4B. After incubation for 2 h at 4°C, the beads were washed five times with lysis buffer, and bound proteins were resolved by SDS-PAGE and visualized by Coomassie brilliant blue (CBB). The bands of interest were identified by mass spectrometry.

Immunofluorescence microscopy

Cells were fixed with 3.7% formaldehyde in PBS for 10 min at RT and were then permeabilized with PBS containing 0.2% Triton X-100 for 5 min at RT, washed three times with PBS, and blocked with Image-iT FX signal enhancer (Invitrogen) for 30 min at RT. Cells were incubated with primary antibodies in PBS for 90 min. After three washes with PBS, cells were incubated with the appropriate secondary antibodies in PBS for 1 h. After a brief wash with PBS, coverslips were mounted onto slides using PermaFluor Mountant Medium (Thermo Fisher Scientific) and observed under a Fluoview 1000-D confocal microscope (IX81; Olympus) equipped with 473-, 568-, and 633-nm diode lasers (Olympus) through an objective lens (60 \times oil immersion objective, NA 1.35; Olympus) and with Fluoview software (Olympus). Acquired images were processed with Photoshop (Adobe).

Live cell imaging

NIH3T3 cells transfected with the indicated constructs were grown on glass-base dishes (Iwaki America). Cells were starved in serum-free DME for 16 h and then imaged in the same medium before and after the addition

of PDGF (final, 20 ng/ml). The images were acquired for 10–15 min at 15-s intervals by using a Fluoview 1000-D confocal microscope through an objective lens (60 \times oil immersion objective, NA 1.35) at RT.

Liposome cosedimentation assay

Brain lipids (Folch fraction I; Sigma-Aldrich) or mixtures of PE (70%), PC (20%), and 10% of various acidic phospholipids were dried under nitrogen gas and then suspended in 50 μ l of buffer (25 mM Hepes, pH 7.5, 100 mM NaCl, and 0.5 mM EDTA) for 1 h at 37°C to allow formation of liposomes. Before mixing with the liposomes, proteins were subjected to centrifugation at 150,000 g for 15 min at 4°C to remove aggregated portions. Proteins that came to the supernatant (5 μ g) were incubated with the liposomes (25 μ g) for 15 min at RT and centrifuged at 150,000 g for 20 min at 20°C. Proteins that sedimented with liposomes in the pellet and unbound proteins in the supernatant were separated and then subjected to SDS-PAGE followed by CBB staining.

F-actin binding assay

Rabbit skeletal muscle actin (Cytoskeleton) in G buffer (2 mM Tris, pH 8.0, 0.1 mM CaCl₂, 0.2 mM ATP, and 0.5 mM DTT) was first subjected to a centrifugation at 180,000 g for 10 min at 4°C. The supernatant (G actin) was incubated in polymerization buffer (2 mM Tris, pH 8.0, 50 mM KCl, 2 mM ATP, and 2 mM MgCl₂) for 1 h at RT to form F-actin. Purified recombinant proteins were centrifuged at 180,000 g for 10 min at 4°C, and then 5 μ g of proteins was incubated with 4 μ M F-actin for 30 min at RT and centrifuged at 180,000 g for 20 min at 4°C. Proteins in pellet and supernatant were visualized by CBB staining.

Phosphoinositides overlay assay

To label PH domains, pGEX-6P-3-6xCys was constructed by inserting an oligonucleotide (5'-TGCTGCTGCTGCTGCTG-3') into pGEX-6P-3. Each PH domain sequence (Grp1PH, 2xTapp1PH, and PLC δ 1PH) was inserted into this vector, and recombinant proteins were obtained as described in the previous section. The six tandem cysteine residues at the N terminus of each PH domain were labeled with the Qdot (585, 655, and 707) antibody conjugation kit (Invitrogen). Cellular lipids were extracted as previously described (Gray et al., 2003). In brief, cells were scraped with 0.5 M trichloroacetate solution and then incubated with chloroform/methanol (1:2, vol/vol) to remove neutral lipids. The acidic lipids were extracted from the remaining pellets by incubating with chloroform/methanol/HCl (40:80:1, vol/vol/vol). Extracted acidic lipids were dried under nitrogen gas, suspended in chloroform, and then spotted onto nitrocellulose membrane (5 μ g each). The membrane was incubated in a blocking buffer (PBS containing 5% skim milk, 1% BSA, and 0.05% Tween 20) for 45 min and then probed with 100 μ g/ml Qdot-labeled PH domains in PBS containing 0.05% Tween 20. After 2 h, membranes were washed three times and quantified by a fluorescent image analyzer (FLA-8000; Fujifilm).

RT-PCR

RT-PCR analysis was performed using these primers (5'-GTCACTACCC-CTCTCTTCAACTTC-3' and 5'-GGCTATCCAGGTAGCCTCATACT-3') for mouse PI3K-C2 β cDNA.

Statistical analysis

Statistically significant differences were determined using the Student's *t* test. Differences were considered significant if *P* < 0.05.

Online supplemental material

Fig. S1 shows the evolutionary conservation of SYLF domains and their F-actin binding properties. Fig. S2 shows lipid-binding specificity and dorsal ruffle localization of the SYLF domain-only constructs. Fig. S3 shows that PI3K-C2 β and Tapp1 are localized at, as well as required for the formation of, circular dorsal ruffles. Fig. S4 shows the appearances of SH3YL1, SHIP2, PI(3,4)P₂, PI(3,4,5)P₃, and F-actin at dorsal ruffles revealed by time-lapse microscopy. Fig. S5 shows a dot-blot assay for quantifying phosphoinositide levels after PDGF stimulation. Online supplemental material is available at <http://www.jcb.org/cgi/content/full/jcb.201012161/DC1>.

We are grateful to Takehiko Sasaki, Shusaku Kurisu, and Yasunori Yamamoto for materials, Naoya Hatano and Yasuhiro Iriki for technical assistance, and Hiroyuki Arai, Takao Inoue, Yohko Tanaka-Takiguchi, and Kingo Takiguchi for discussions.

This study was supported in part by a Grant-in-Aid for Creative Scientific Research from the Japan Society for the Promotion of Science (JSPS) to T. Takenawa and T. Itoh, a Grant-in-Aid for Young Scientists from the JSPS to T. Itoh, and Global Centers of Excellence Program grants from the JSPS to J. Hasegawa, H. Hiroaki, T. Takenawa, and T. Itoh.

References

Aoki, N., K. Ito, and M. Ito. 2000. A novel mouse gene, Sh3yl1, is expressed in the anagen hair follicle. *J. Invest. Dermatol.* 114:1050–1056. doi:10.1046/j.1523-1747.2000.00971.x

Araki, N., M.T. Johnson, and J.A. Swanson. 1996. A role for phosphoinositide 3-kinase in the completion of macropinocytosis and phagocytosis by macrophages. *J. Cell Biol.* 135:1249–1260. doi:10.1083/jcb.135.5.1249

Bhatia, V.K., K.L. Madsen, P.Y. Bolinger, A. Kunding, P. Hedegård, U. Gether, and D. Stamou. 2009. Amphipathic motifs in BAR domains are essential for membrane curvature sensing. *EMBO J.* 28:3303–3314. doi:10.1038/emboj.2009.261

Buccione, R., J.D. Orth, and M.A. McNiven. 2004. Foot and mouth: podosomes, invadopodia and circular dorsal ruffles. *Nat. Rev. Mol. Cell Biol.* 5:647–657. doi:10.1038/nrm1436

Buschman, M.D., P.A. Bromann, P. Cejudo-Martin, F. Wen, I. Pass, and S.A. Courtneidge. 2009. The novel adaptor protein Tks4 (SH3PXD2B) is required for functional podosome formation. *Mol. Biol. Cell.* 20:1302–1311. doi:10.1091/mbc.E08-09-0949

Dewar, H., D.T. Warren, F.C. Gardiner, C.G. Gourlay, N. Satish, M.R. Richardson, P.D. Andrews, and K.R. Ayscough. 2002. Novel proteins linking the actin cytoskeleton to the endocytic machinery in *Saccharomyces cerevisiae*. *Mol. Biol. Cell.* 13:3646–3661. doi:10.1091/mbc.E02-05-0262

Dharmawardhane, S., A. Schürmann, M.A. Sells, J. Chernoff, S.L. Schmid, and G.M. Bokoch. 2000. Regulation of macropinocytosis by p21-activated kinase-1. *Mol. Biol. Cell.* 11:3341–3352.

Dowrick, P., P. Kenworthy, B. McCann, and R. Warn. 1993. Circular ruffle formation and closure lead to macropinocytosis in hepatocyte growth factor/scatter factor-treated cells. *Eur. J. Cell Biol.* 61:44–53.

Dyson, J.M., C.J. O’Malley, J. Becanovic, A.D. Munday, M.C. Berndt, I.D. Coghill, H.H. Nandurkar, L.M. Ooms, and C.A. Mitchell. 2001. The SH2-containing inositol polyphosphate 5-phosphatase, SHIP-2, binds filamin and regulates submembraneous actin. *J. Cell Biol.* 155:1065–1079. doi:10.1083/jcb.200104005

Ebina, T., H. Toh, and Y. Kuroda. 2009. Loop-length-dependent SVM prediction of domain linkers for high-throughput structural proteomics. *Biopolymers*. 92:1–8. doi:10.1002/bip.21105

Emanuelsson, O., S. Brunak, G. von Heijne, and H. Nielsen. 2007. Locating proteins in the cell using TargetP, SignalP and related tools. *Nat. Protoc.* 2:953–971. doi:10.1038/nprot.2007.131

Farsad, K., N. Ringstad, K. Takei, S.R. Floyd, K. Rose, and P. De Camilli. 2001. Generation of high curvature membranes mediated by direct endophilin bilayer interactions. *J. Cell Biol.* 155:193–200. doi:10.1083/jcb.200107075

Ford, M.G., I.G. Mills, B.J. Peter, Y. Vallis, G.J. Praefcke, P.R. Evans, and H.T. McMahon. 2002. Curvature of clathrin-coated pits driven by epsin. *Nature*. 419:361–366. doi:10.1038/nature01020

Foster, F.M., C.J. Traer, S.M. Abraham, and M.J. Fry. 2003. The phosphoinositide (PI) 3-kinase family. *J. Cell Sci.* 116:3037–3040. doi:10.1242/jcs.00609

Gaidarov, I., M.E. Smith, J. Domin, and J.H. Keen. 2001. The class II phosphoinositide 3-kinase C2alpha is activated by clathrin and regulates clathrin-mediated membrane trafficking. *Mol. Cell.* 7:443–449. doi:10.1016/S1097-2765(01)00191-5

Gallop, J.L., C.C. Jao, H.M. Kent, P.J. Butler, P.R. Evans, R. Langen, and H.T. McMahon. 2006. Mechanism of endophilin N-BAR domain-mediated membrane curvature. *EMBO J.* 25:2898–2910. doi:10.1038/sj.emboj.7601174

Gewinner, C., Z.C. Wang, A. Richardson, J. Teruya-Feldstein, D. Etemadmoghadam, D. Bowtell, J. Barretina, W.M. Lin, L. Rameh, L. Salmena, et al. 2009. Evidence that inositol polyphosphate 4-phosphatase type II is a tumor suppressor that inhibits PI3K signaling. *Cancer Cell*. 16:115–125. doi:10.1016/j.ccr.2009.06.006

Gray, A., H. Olsson, I.H. Batty, L. Priganica, and C. Peter Downes. 2003. Nonradioactive methods for the assay of phosphoinositide 3-kinases and phosphoinositide phosphatases and selective detection of signaling lipids in cell and tissue extracts. *Anal. Biochem.* 313:234–245. doi:10.1016/S0003-2697(02)00607-3

Heath, R.J., and R.H. Insall. 2008. F-BAR domains: multifunctional regulators of membrane curvature. *J. Cell Sci.* 121:1951–1954. doi:10.1242/jcs.023895

Hogan, A., Y. Yakubchik, J. Chabot, C. Obagi, E. Daher, K. Maekawa, and S.H. Gee. 2004. The phosphoinositol 3,4-bisphosphate-binding protein TAPP1 interacts with syntrophins and regulates actin cytoskeletal organization. *J. Biol. Chem.* 279:53717–53724. doi:10.1074/jbc.M410654200

Ishihara, H., T. Sasaoka, H. Hori, T. Wada, H. Hirai, T. Haruta, W.J. Langlois, and M. Kobayashi. 1999. Molecular cloning of rat SH2-containing inositol phosphatase 2 (SHIP2) and its role in the regulation of insulin signaling. *Biochem. Biophys. Res. Commun.* 260:265–272. doi:10.1006/bbrc.1999.0888

Itoh, T., and P. De Camilli. 2006. BAR, F-BAR (EFC) and ENTH/ANTH domains in the regulation of membrane–cytosol interfaces and membrane curvature. *Biochim. Biophys. Acta.* 1761:897–912.

Itoh, T., and T. Takenawa. 2002. Phosphoinositide-binding domains: functional units for temporal and spatial regulation of intracellular signalling. *Cell. Signal.* 14:733–743. doi:10.1016/S0898-6568(02)00028-1

Itoh, T., K.S. Erdmann, A. Roux, B. Habermann, H. Werner, and P. De Camilli. 2005. Dynamin and the actin cytoskeleton cooperatively regulate plasma membrane invagination by BAR and F-BAR proteins. *Dev. Cell.* 9:791–804. doi:10.1016/j.devcel.2005.11.005

Juncker, A.S., H. Willenbrock, G. Von Heijne, S. Brunak, H. Nielsen, and A. Krogh. 2003. Prediction of lipoprotein signal peptides in Gram-negative bacteria. *Protein Sci.* 12:1652–1662. doi:10.1110/ps.0303703

Kamioka, Y., S. Fukuhara, H. Sawa, K. Nagashima, M. Masuda, M. Matsuda, and N. Mochizuki. 2004. A novel dynamin-associating molecule, formin-binding protein 17, induces tubular membrane invaginations and participates in endocytosis. *J. Biol. Chem.* 279:40091–40099. doi:10.1074/jbc.M40499200

Kang, H., C. Freund, J.S. Duke-Cohan, A. Musacchio, G. Wagner, and C.E. Rudd. 2000. SH3 domain recognition of a proline-independent tyrosine-based RKxxYxxY motif in immune cell adaptor SKAP55. *EMBO J.* 19:2889–2899. doi:10.1093/emboj/19.12.289

Krueger, E.W., J.D. Orth, H. Cao, and M.A. McNiven. 2003. A dynamin–cortactin–Arp2/3 complex mediates actin reorganization in growth factor-stimulated cells. *Mol. Biol. Cell.* 14:1085–1096. doi:10.1091/mbc.E02-08-0466

Lanzetti, L., A. Palamidessi, L. Areces, G. Scita, and P.P. Di Fiore. 2004. Rab5 is a signalling GTPase involved in actin remodelling by receptor tyrosine kinases. *Nature*. 429:309–314. doi:10.1038/nature02542

Lee, E., M. Marcucci, L. Daniell, M. Pypaert, O.A. Weisz, G.C. Ochoa, K. Farsad, M.R. Wenk, and P. De Camilli. 2002. Amphiphysin 2 (Bin1) and T-tubule biogenesis in muscle. *Science*. 297:1193–1196. doi:10.1126/science.1071362

Legg, J.A., G. Bompard, J. Dawson, H.L. Morris, N. Andrew, L. Cooper, S.A. Johnston, G. Tramontanai, and L.M. Machesky. 2007. N-WASP involvement in dorsal ruffle formation in mouse embryonic fibroblasts. *Mol. Biol. Cell.* 18:678–687. doi:10.1091/mbc.E06-06-0569

Lemmon, M.A. 2008. Membrane recognition by phospholipid-binding domains. *Nat. Rev. Mol. Cell Biol.* 9:99–111. doi:10.1038/nrm2328

Liu, Y.W., M.C. Surka, T. Schroeter, V. Lukiyanchuk, and S.L. Schmid. 2008. Isoform and splice-variant specific functions of dynamin-2 revealed by analysis of conditional knock-out cells. *Mol. Biol. Cell.* 19:5347–5359. doi:10.1091/mbc.E08-08-0890

Mayer, B.J., and R. Gupta. 1998. Functions of SH2 and SH3 domains. *Curr. Top. Microbiol. Immunol.* 228:1–22.

McMahon, H.T., and J.L. Gallop. 2005. Membrane curvature and mechanisms of dynamic cell membrane remodelling. *Nature*. 438:590–596. doi:10.1038/nature04396

Mellström, K., C.H. Heldin, and B. Westermark. 1988. Induction of circular membrane ruffling on human fibroblasts by platelet-derived growth factor. *Exp. Cell Res.* 177:347–359. doi:10.1016/0014-4827(88)90468-5

Oikawa, T., T. Itoh, and T. Takenawa. 2008. Sequential signals toward podosome formation in NIH-src cells. *J. Cell Biol.* 182:157–169. doi:10.1083/jcb.200801042

Orth, J.D., and M.A. McNiven. 2006. Get off my back! Rapid receptor internalization through circular dorsal ruffles. *Cancer Res.* 66:11094–11096. doi:10.1158/0008-5472.CAN-06-3397

Palamidessi, A., E. Frittoli, M. Garré, M. Faretta, M. Mione, I. Testa, A. Diaspro, L. Lanzetti, G. Scita, and P.P. Di Fiore. 2008. Endocytic trafficking of Rac is required for the spatial restriction of signaling in cell migration. *Cell*. 134:135–147. doi:10.1016/j.cell.2008.05.034

Riedl, J., A.H. Crevenna, K. Kessenbrock, J.H. Yu, D. Neukirchen, M. Bista, F. Bradke, D. Jenne, T.A. Holak, Z. Werb, et al. 2008. Lifeact: a versatile marker to visualize F-actin. *Nat. Methods*. 5:605–607. doi:10.1038/nmeth.1220

Ringstad, N., Y. Nemoto, and P. De Camilli. 1997. The SH3p4/Sh3p8/Sh3p13 protein family: binding partners for synaptotagmin and dynamin via a Grb2-like Src homology 3 domain. *Proc. Natl. Acad. Sci. USA*. 94:8569–8574. doi:10.1073/pnas.94.16.8569

Robertson, A.S., E.G. Allwood, A.P. Smith, F.C. Gardiner, R. Costa, S.J. Winder, and K.R. Ayscough. 2009. The WASP homologue Las17 activates the

novel actin-regulatory activity of Ysc84 to promote endocytosis in yeast. *Mol. Biol. Cell.* 20:1618–1628. doi:10.1091/mbc.E08-09-0982

Sasaki, J., S. Kofuji, R. Itoh, T. Momiyama, K. Takayama, H. Murakami, S. Chida, Y. Tsuya, S. Takasuga, S. Eguchi, et al. 2010. The PtdIns(3,4)P₂ phosphatase INPP4A is a suppressor of excitotoxic neuronal death. *Nature*. 465:497–501. doi:10.1038/nature09023

Schlunck, G., H. Damke, W.B. Kiosses, N. Rusk, M.H. Symons, C.M. Waterman-Storer, S.L. Schmid, and M.A. Schwartz. 2004. Modulation of Rac localization and function by dynamin. *Mol. Biol. Cell.* 15:256–267. doi:10.1091/mbc.E03-01-0019

Sindić, A., A. Aleksandrova, A.P. Fields, S. Volin, and H. Banfić. 2001. Presence and activation of nuclear phosphoinositide 3-kinase C2beta during compensatory liver growth. *J. Biol. Chem.* 276:17754–17761. doi:10.1074/jbc.M006533200

Suetsugu, S., D. Yamazaki, S. Kurisu, and T. Takenawa. 2003. Differential roles of WAVE1 and WAVE2 in dorsal and peripheral ruffle formation for fibroblast cell migration. *Dev. Cell.* 5:595–609. doi:10.1016/S1534-5807(03)00297-1

Suyama, M., and O. Ohara. 2003. DomCut: prediction of inter-domain linker regions in amino acid sequences. *Bioinformatics*. 19:673–674. doi:10.1093/bioinformatics/btg031

Swanson, J.A., and C. Watts. 1995. Macropinocytosis. *Trends Cell Biol.* 5:424–428. doi:10.1016/S0962-8924(00)89101-1

Takei, K., V.I. Slepnev, V. Haucke, and P. De Camilli. 1999. Functional partnership between amphiphysin and dynamin in clathrin-mediated endocytosis. *Nat. Cell Biol.* 1:33–39. doi:10.1038/9004

Tsujita, K., S. Suetsugu, N. Sasaki, M. Furutani, T. Oikawa, and T. Takenawa. 2006. Coordination between the actin cytoskeleton and membrane deformation by a novel membrane tubulation domain of PCH proteins is involved in endocytosis. *J. Cell Biol.* 172:269–279. doi:10.1083/jcb.200508091

Warn, R., D. Brown, P. Dowrick, A. Prescott, and A. Warn. 1993. Cytoskeletal changes associated with cell motility. *Symp. Soc. Exp. Biol.* 47:325–338.

Xie, J., I. Vandebroere, and I. Pirson. 2008. SHIP2 associates with intersectin and recruits it to the plasma membrane in response to EGF. *FEBS Lett.* 582:3011–3017. doi:10.1016/j.febslet.2008.07.048

Yarar, D., C.M. Waterman-Storer, and S.L. Schmid. 2007. SNX9 couples actin assembly to phosphoinositide signals and is required for membrane remodeling during endocytosis. *Dev. Cell.* 13:43–56. doi:10.1016/j.devcel.2007.04.014